Designing and Testing Model Systems for Catalysis
- monomers, dimers and clusters

Ph.D. Thesis

Karl Krøjer Toudahl

Supervisor: Professor Jakob Doganli-Kibsgaard
Co-supervisor: Professor Ib Chorkendorff

Technical University of Denmark
Department of Physics
Surface Physics and Catalysis (SurfCat)
March 2023

Abstract

The great challenge of the 21st century is to deliver cheap and green energy to the growing world population. Some sectors will be difficult to decarbonize by electrification and requires the use of chemicals. Hydrogen produced through acidic water splitting can be used as feedstock for chemical processes and as an energy carrier to alleviate the intermittency of renewables. In order for water splitting to become viable, alternative catalysts are needed. Furthermore, a better understanding of catalysis as a whole is needed to accelerate the discovery of new catalyst materials. This thesis explores catalytic model systems with low complexity to further our understanding and improve the methods used to explore new catalysts.

Benchmarking the hydrogen evolution reaction: Current experimental practices within the field of hydrogen evolution suffer from several pitfalls. Through the systematic analysis of a wide range of Pt catalyst loadings, mass transport limitations in the rotating disk electrode (RDE) setup are shown to be ubiquitous for acidic HER. The consequence is that the true catalyst activity of Pt is still unknown but is three orders of magnitude higher than earth abundant alternatives. A strategy of reduced catalyst loading is suggested to mitigate mass transport limitations in RDE and the best experimental practices are highlighted.

Small entities for the hydrogen evolution reaction: Small entities i.e. monomers, dimers and trimers are existing new catalyst candidates. Dimers and trimers are especially difficult to synthesize chemically and literature reports on the subject are sparse within hydrogen evolution. By the use of a cluster source deposition technique Pt monomers and dimers were investigated for the hydrogen evolution reaction. The atomic structure of the deposited entities could not be confirmed, but the catalytic activity was found to be markedly worse than Pt nanoparticles.

Resumé

Den store udfordring i det 21. århundrede er at levere billig og grøn energi til den voksende verdensbefolkning. Nogle sektorer vil være svære at afkarbonisere ved hjælp af elektrificering og kræver brug af kemikalier. Hydrogen produceret gennem sur vandspaltning kan bruges som feedstock til kemiske processer og som en energibærer for at afhjælpe afbrydelser af energiforsyningen forbundet med vedvarende energikilder. For at vandspaltning kan blive levedygtig, er alternative katalysatorer nødvendige. Derudover er en bedre forståelse af katalyse som helhed nødvendig for at fremskynde opdagelsen af nye katalysatorer. Denne afhandling udforsker katalytiske modelsystemer med lav kompleksitet for at forbedre vores forståelse og forbedre metoderne, der bruges til at undersøge nye katalysatorer.

Benchmark af hydrogenudvikling: Nuværende eksperimentiel praksis inden for området for hydrogenudvikling lider af flere problemer. Gennem systematisk analyse af et bredt spektrum af Pt katalysator mængder vises det, at masstransportbegrænsninger i den roterende disk elektrode (RDE) opsætning er allestedsværende for sur HER. Konsekvensen er, at den sande aktivitet for Pt stadig er ukendt, men er tre størrelsesordener højere end ikke-noble alternativer. En strategi med reduceret katalysatormængde foreslås for at afhjælpe masstransportbegrænsninger i RDE og de bedste eksperimentelle praksis fremhæves.

Små enheder til hydrogenudvikling: Små enheder, dvs. monomerer, dimere og trimere, er spændende nye katalysator-kandidater. Dimere og trimere er især svære at syntetisere kemisk, og litteraturrapporter om emnet er sjældne inden for hydrogenudvikling. Ved brug af en klyngekilde depositionsteknik undersøges Pt monomerer og dimere til hydrogenudviklingsreaktionen. Den atomare struktur af de deponerede enheder kunne ikke bekræftes, men den katalytiske aktivitet viste sig at være markant ringere end Pt nanopartikler.

Preface

This thesis is submitted in partial fulfillment of the requirements for the Ph.D. degree from the Technical University of Denmark. The work presented in this thesis was conducted under the supervision of Professor Jakob Doganli-Kibsgaard and Professor Ib Chorkendorff in connection to the Single Atom Site project, funded by the Carlsberg Foundation. The work took place from September 2019 until March 2023 in the Surface Physics & Catalysis (SurfCat) group, Department of Physics, Technical University of Denmark.

It has truly been a great learning experience, extremely challenging and a lot of fun working in the SurfCat group. I want to thank my supervisors Professors Jakob and Ib for your sparring, guidance and ambition on my behalf. Throughout my time at SurfCat I have had the pleasure of working with the best brains and personalities science has to offer. I want to thank Niklas Secher and Johannes Hartmann for introducing me to the small entity project and for initializing the project as a whole. I want to thank Jakob Ejler for assisting me whenever my UHV troubleshooting skillset was inadequate. As time went on and people graduated new faces joined the ranks of the cluster source batallion. I want to thank Julius Needham for his sparring and good times in the cluster source lab. Thank you to Alexander Juul Nielsen for giving feedback on the thesis and thank you to Louise Lemming and Tor Toudahl for checking my spelling. A special thanks goes to Rikke Tankard and Chao Wei for your work with me on the small entity project; I could not have done this without you. I also want to thank Peder Heise and Dan Shacham of the workshop for fabricating sample holder and TPD stage used in the project.

Last but not least I want to thank my partner Caroline Lauritsen for listening to my frustrations and for taking care of our daughter during this final and intensive writing spree.

Contents

List of Figures

List of Tables

Appended Paper

Paper I

Is There Anything Better Than Pt For HER?
Johannes Novak Hansen, Hector Prats, Karl Krøjer Toudahl, Niklas Mørch Secher, Karen Chan, Jakob Kibsgaard, Ib Chorkendorff
ACS Energy Letters, Volume 6, 2021, Pages 1175-1180

`http://pubs.acs.org/doi/10.1021/acsenergylett.1c00246`

Chapter 1

Introduction

The introduction aims to motivate the scientific studies presented in the thesis. I will not spend much time on the need to replace fossil fuels as it finally seems to be widely agreed upon. I will briefly introduce catalysis and electrocatalysis to set the stage for the model systems investigated in later chapters.

1.1 The terawatt challenge

In 2005, shortly before his untimely death, American chemist Richard E. Smalley published an article in *MRS Bulletin* called "Future Global Energy Prosperity: The Terawatt Challenge".[1] In this article, Smalley argues that the biggest challenge of the 21st century is securing an abundant and cheap energy resource. Since the industrial revolution, humanity has experienced a steady increase in standard of living through technological advances; all enabled by the burning of fossil fuels. Fossil fuels have been an amazing energy resource, but it is finite. The growing world population and the desire to make cheap energy resources available to developing nations, means fossil fuels are not a sustainable energy resource.[2] Furthermore, the burning of fossil fuels have significantly altered the atmosphere and we are now in a race against time to decarbonize our energy supply.[3]

The terawatt challenge got its name from the power needed to supply the global energy demand, currently 18:6 TW.[4] Luckily, a huge fusion reactor 150 10^6 km away continuously supplies our planet with a power input of

165 000 TW.[1] As solar panels and wind turbines are now cost competitive it is 'simply' a matter of implementing these technologies at scale.[5] There are two caveats: First, the energy generated from renewables comes in the form of electricity and second the intermittent nature of renewables. At present, only 15 % of the global energy mix stems of electrical energy consumption,[6] meaning electrification will be a huge part of the green transition. However, some industries will be difficult to electrify such as commercial transportation, which accounts for 1.8 TW of global power use.[4] Chemicals are more suited in these applications. Figure 1.1 shows the energy demand in Denmark over a two week period in May 2015. The supply and demand do not always match, which gives rise to an energy storage need. This need will still be there as the renewables resources are increased, as evident from the shaded blue area in figure 1.1.

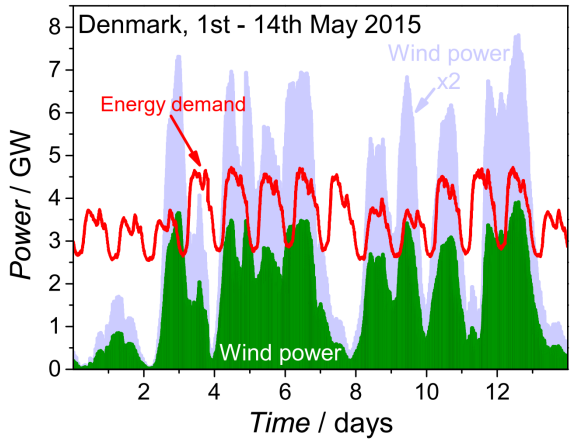

Figure 1.1: Energy demand and windpower supply for a two week period in Denmark. Data from,[7] figure reprinted from.[8]

These observations motivate the need for a new energy infrastructure where fossil fuels are no longer the primary energy vector.

1.1.1 A sustainable energy infrastructure

Figure 1.2 shows an alternative sustainable energy infrastructure, where energy in the form of electricity is generated through wind, solar and hydro power. The idea is then to generate fuels and chemicals through elec-

trochemical reactions, i.e. reactions where the driving force is an electric potential. This makes it possible to generate the resources that cannot be solved by electrification. Splitting water into H_2 and O_2 allows H_2 to be stored under pressure and act as an energy carrier. Combining H_2 and O_2 in a fuel cell allows for electricity generation on demand. Furthermore, hydrogen can be used as feedstock for other vital chemical reactions such as the the Haber-Bosch process.

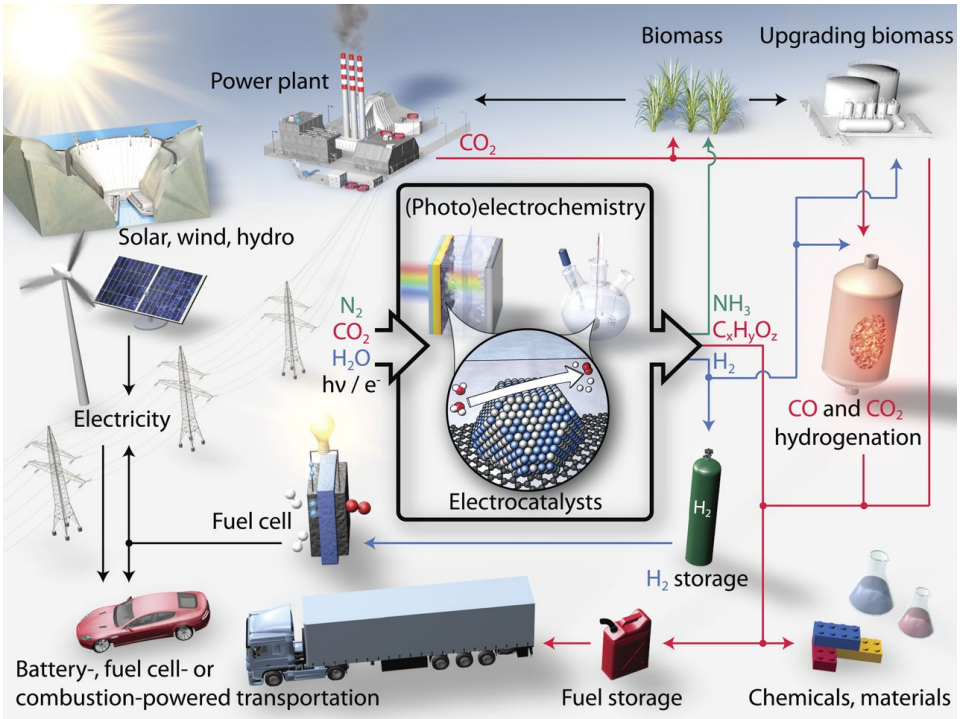

Figure 1.2: A sustainable energy infrasture, which of course has catalysis at its center. Figure reprinted with permission from.[4]

In order to make these reactions economically viable, a catalyst is needed to increase the reaction rate and make the chemistry more efficient.[4]

1.2 Catalysis

Catalysis is at the core of modern society, with 90% of industrial chemical reactions requiring a catalyst to be viable.[9] A catalyst increases the rate of a chemical reaction without being spent. In heterogeneous catalysis, the catalyst is typically a solid material, whereas the reactants and products exist in a liquid of gaseous phase. This allows for easy collection of the desired product.

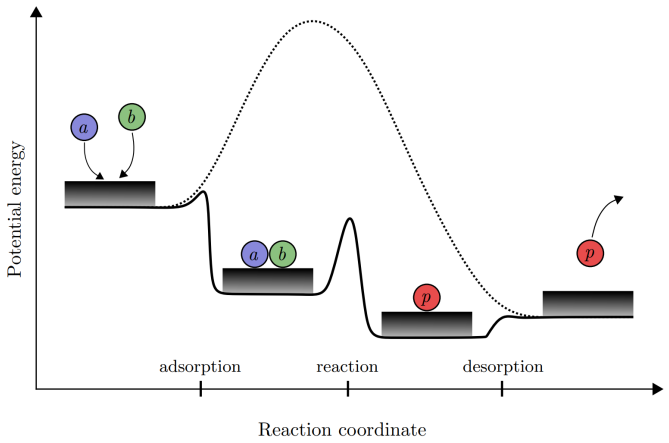

Figure 1.3: Schematic illustration of a catalysed (black) and uncatalysed (stippled) chemical reaction pathway. Image courtesy of Johannes Novak Hartmann.

Figure 1.3 shows a catalysed (black) and uncatalysed (stippled) chemical reaction pathway. The reactants A and B can react to form the product P by collision, but at a slow rate due to the large potential energy barrier. By adsorbing on the catalyst they are offered an alternative reaction pathway with lower energy barriers, which greatly increases the rate of reaction. The product P is then released from the catalyst surface. In order for the catalyst to be optimal, there must exist a balance between the adsorption and desorption energies. If the reactants bind too strongly, they will poison the catalyst and never from product. If they bind too weakly, they will not adsorb on the catalyst. This balance is called the Sabatier principle.

1.2.1 Electrocatalysis

In electrocatalysis, an electrical potential is used as driving force for the electrochemical reaction in question. These processes require the transfer of electrons through oxidation and reduction of the participating reactants. In practise the oxidation and reduction reactions happen at an electrode where the electrocatalyst is present. By applying a negative potential to the electrode the energy of the electrons are increased, which favors transfer of electrons to the reduced species i.e. reduction. Conversely, applying a positive potential decreases the energy of the electrons and favors oxidation.

The Nernst equation relates the potential of an electrochemical cell to the standard cell potential and the concentration of the reduced and oxidized species, formally

$$E = E^0 + \frac{RT}{n\mathcal{F}} \ln \frac{[O]}{[R]} \tag{1.1}$$

where E^0 is the standard potential, R is the gas constant, T is the temperature, n is the number of electrons being transferred, $\mathcal{F}$ is Faraday's constant, [O] is the concentration of the oxidized species and [R] is the concentration of the reduced species. The standard potential is the thermodynamically determined potential under standard conditions of the redox couple taking part in the reaction.

From equation 1.1, it is clear that $E = E^0$, whenever the concentration of the reduced and oxidized species is equal. Thereby, in order to drive the reaction towards more product, E must be altered. The efficiency of an electrochemical cell is determined by the overpotential h, which is a metric of the additional voltage required to drive the reaction, as compared to the thermodynamically determined potential. The total overpotential of the cell can be split into its constituent contributors, such as the ohmic resistance, mass transport limitations and reaction kinetics. The overpotential is given as

$$h = E_{\text{applied}} \quad E_{\text{eq}} \tag{1.2}$$

where E_{eq} is given from the Nernst equation 1.1 and E_{applied} is the potential, which is applied in practise. By this notion, reducing the overpotential for an electrochemical reaction is the goal of the electrocatalyst.

1.2.2 The hydrogen evolution reaction

The simplest electrochemical reaction is the combinations of protons and electrons to form molecular hydrogen. This process happens in the proton exhange membrane water electrolyzer (PEMWE), where water is oxidized to generate protons, which travel through the membrane and combines with electrons to form hydrogen. This happens in an acidic environment. Thereby, splitting water requires two half reactions which are given as

$$4H^+ + 4e \underset{\text{HOR}}{\overset{\text{HER}}{\rightleftharpoons}} 2H_2 \qquad E^0 = 0 \text{ vs. RHE}$$

$$2H_2O \underset{\text{ORR}}{\overset{\text{OER}}{\rightleftharpoons}} O_2 + 4H^+ + 4e \qquad E^0 = 1.23 \text{ vs. RHE}$$

The RHE (revsersible hydrogen electrode) has not been formally introduced yet and will be discussed in section 2.4.1. Here the HER denoted the hydrogen evolution reaction, HOR is the hydrogen oxidation reaction, OER is the oxygen evolution reaction and ORR is the oxygen reduction reaction.

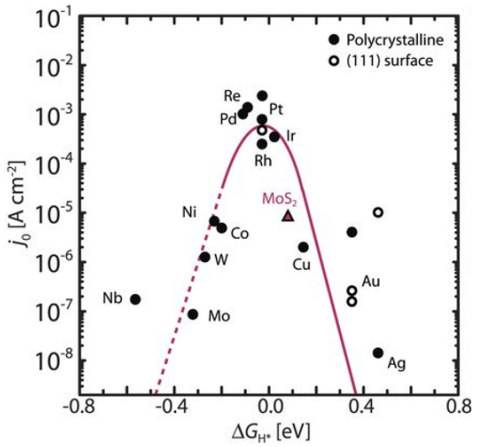

Figure 1.4: Measured current densities for different HER catalysts using the binding energy of protons to explain the activity trend. Figure reprinted from[4] with permission.

In the field of water splitting the name evolution may replace 'oxidation' or 'reduction' and 'proton reduction' is instead named hydrogen evolution, whereas 'water oxidation' is named oxygen evolution.
One of the great findings in electrocatalysis in the past decades[10] is the rationalization of the measured HER catalyst activities using the Sabatier principle shown in figure 1.4. Using the binding energy of DG_{H^+} as a descriptor, catalysts with DG_{H^+} 0 show the highest activity. The values of DG_{H^+} for a material is calculated using density functional theory (DFT), where the electronic structure of a material is approximated by the density of electrons. Pt sits on top of the activity volcano and remains the best HER catalyst.

1.2.3 The need for catalytic model systems

Discovering a catalyst, which is suitable for industrial level production of chemicals is no easy task. While attempting to scale up of nitrogen fixation to ammonia, it took Bosch's assistant, chemist Alwin Mittasch and his team, a screening of 20000 samples and later testing 2500 different catalyst mixes to perfect a catalyst based on iron oxide still used today.[11;12] Within acidic water splitting, no one has to this day demonstrated catalysts which could replace Pt for HER or IrO_x for OER in a real device. This poses a challenge, as both elements - but especially Ir - are scarce and hinder the TW scale deployment of PEMWEs.[13] When searching for a new catalyst, the central figure of merit is the turnover frequency (TOF), which denotes the number of product molecules evolved per site per unit of time. Even though computational chemistry has seen huge advances in the past decades, it remains a central challenge to accurately predict the turnover frequency of a candidate catalyst. Consider the following example, where TOF is given as

$$\text{TOF} = A\exp \quad \frac{E_a}{kT} \tag{1.3}$$

where A is a prefactor, E_a is the energy barrier, k is the Boltzmann constant and T is the temperature. Current DFT methods in vacuum yield errors of 0.15 eV,[14] which translates to a factor of 400 difference in turnover frequency. Introducing a liquid environment present in electrochemistry compounds this error as there currently is no accurate way to account for the

electrolyte computationally.[14] To this end, the error of the DFT method approaches 100 % wrt. selectivity. This does not take stability into account. Therefore it is absolutely essential to bridge the gap between the experimental and computational results, unless we want to stick with trial and error as Alwin and his colleagues.

A catalytic model system seeks to reduce the complexity of the overall catalytic interface to yield unambiguous, accurate and precise results. These experimental findings can then hopefully function as benchmarks for the computational methods.

1.3 Thesis structure

Having motivated the need for new catalysts I will briefly explain the structure of the thesis.

Chapter 1 - introduction: This chapter motivates the need for new catalysts and explains the fundamental principles of catalysis and basic electrochemistry.

Chapter 2 - Experimental methods: This chapter introduces the main experimental methods used in the thesis. Special emphasis will be put on the techniques that I have employed myself. Electrochemical and scanning probe techniques will also be outlined, to explain how the data discussed in later chapters is obtained.

Chapter 3- Benchmarking the hydrogen evolution reaction in acid: This chapter is based on a paper, which was published in *ACS Energy Letters* in 2021 named *Is there anything better than Pt for HER?*. It utilizes a formalism and methods that are then employed to investigate novel catalyst candidates in chapter 4.

Chapter 4 - Small entities for the hydrogen evolution reaction: This chapter contains the main work and the primary focus of my time at SurfCat. Though it is not yet conclusive I aim to show the progress which has been made. Due to the sheer number of experiments and time invested I felt

the need to slice the chapter into three parts. 'Part I - Setting the stage' is a mini literature review, which introduces key literature findings and attempts to challenge and scrutinize the most prevalent papers in the field. 'Part II - Designing and exploring the model system' motivates the need for a model system and explores some of the key findings made throughout my time at SurfCat. 'Part III - Testing the model system' shows the most recent data and the current status of the project. In the epilogue the challenges and opportunities for future work is outlined.

Chapter 5 - Conclusion: This chapter concludes the main points which can be extracted from the thesis as a whole.

Chapter 2

Experimental Methods

2.1 Cluster source deposition

The cluster source is the work horse of the experimental work I have conducted. As the name indicates, it is a source of clusters i.e. nanoparticles or small entities such as single atoms or dimers. Technically, it is a series of connected ultra high vacuum chambers, which have the purpose of generating and filtering the desired cluster or entity. Figure 2.1 shows a cross-sectional view of the cluster source system during deposition.

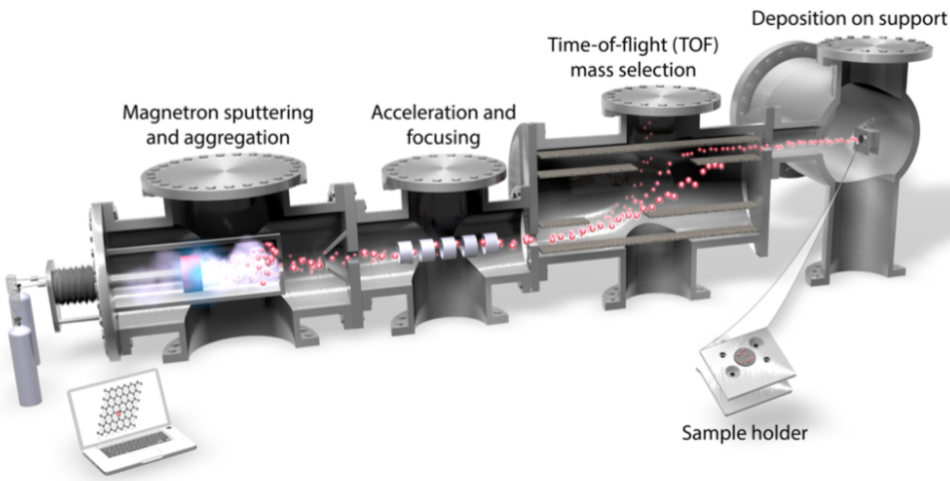

Figure 2.1: cross-sectional view of the cluster source system during deposition. Image courtesy of Jakob Kibsgaard.

The working principle of the cluster source is fairly simple; A metal disc (target) of the desired element is inserted into the aggregation zone on a magnetron sputter head and kept at a negative potential. He and Ar gas is introduced in front of the target which cause the gasses to ionize and accelerate towards the target. This causes a sputtering of the target, ejecting metal atoms into the aggregation zone. Permanent magnets are inserted at the back of the target (magnetron), which confines a plasma of the gasses. This plasma is negatively charged and greatly increases the sputtering rate, while ionizing a large fraction of the ejected metal atoms (now ions). The ejected metal ions can now grow inside the aggregation zone until they escape through a conical 'skimmer' lens and into an electrostatic lens system, which manipulates and focuses the ion beam. After focusing, the ion beam travels into a time-of-flight mass filter. The time-of-flight mass filter generates an electric field (pulse) in the bottom plate, which accelerates the ions based on their mass to charge ratios $\frac{m}{q}$. After a brief time delay an equal and opposite pulse is generated in the top plate. This decelerates the particle beam and causes the particles within the beam to be laterally displaced according to their $\frac{m}{q}$-ratios.[15;16]

The filtered beam exits through an aperture, which may be varied in diameter. The width of this final aperture determines the resolution of the time-of-flight mass filter given as[17]

$$\frac{m_{\text{dep}}}{\Delta m} = [20 \quad 50]$$

with 20 corresponding to the fully open aperture resulting in maximum transmission and minimum resolution. For a 4 nm Pt nanoparticle, this corresponds to an error in size of ± 0.1 nm. One limitation of the time-of-flight mass filter is its inability to distinguish identical mass to charge ratios i.e:

$$\frac{m}{q} = \frac{2m}{2q} = \frac{3m}{3q} \cdots = \frac{Nm}{Nq}$$

Thereby the filtered ion beam is a combination of integer mass to charge ratios. In reality, only the double mass double charge poses an issue. This limiting factor of the mass filter is omitted by 'tuning' the mass distribution such that the double mass ($2M_{\text{dep}}$) is low (< 10) in relative abundance

compared to the desired mass (M_{dep}). The tuning process means changing the conditions in the aggregation zone (gas flow, magnetron power, aggregation zone length) until an acceptable distribution is achieved. Figure 2.2 shows two mass spectra aiming towards 3 and 5 nm Pt nanoparticles.

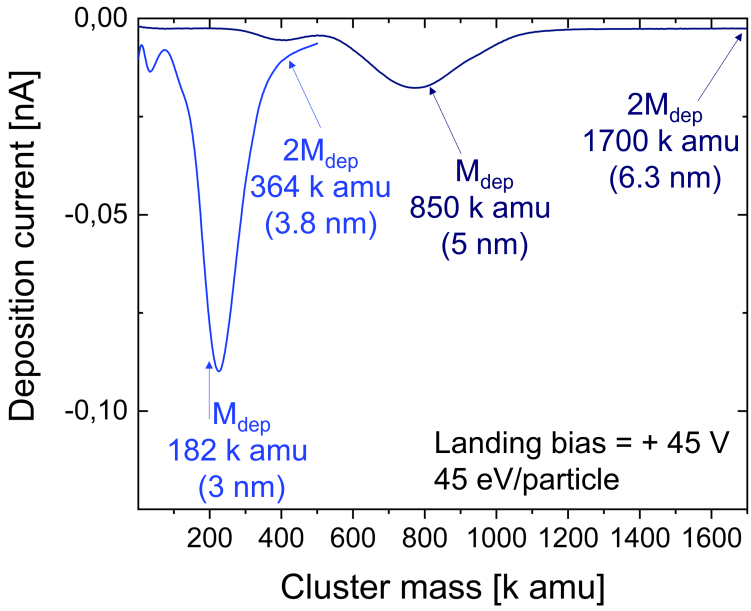

Figure 2.2: Mass spectra of 3 and 5 nm Pt nanoparticles. The conditions in the aggregation zone are tuned to facilitate a high ratio between the desired mass M_{dep} and the double mass $2M_{dep}$.

For these particular sizes, an acceptable deposition current and single to double mass ratio is easily achieved. However, this cluster source system has issues generating a sufficient particle flux of clusters below 1.5 nm and above 10 nm.
When the filtered ion beam is deposited on the desired substrate the neutralization current is measured with an electrometer. As the vast majority of the particles are single charged the number of deposited particles is found as

$$N_{\text{particles}} = \frac{I_{\text{dep}}}{e} \tag{2.1}$$

where $N_{\text{particles}}$ is the deposited number of particles, I_{dep} is the deposition

current, e is the elementary charge and t_{dep} is the time duration of the deposition. Knowing $N_{particles}$ makes it possible to calculate the projected coverage of the nanoparticles or the percentage of single atoms in terms of the target substrate lattice. The target substrate is kept at a potential (landing bias) opposite of the ion beam, which has the effect of guiding and decelerating the ion beam onto the substrate. Since the filtered particles in the ion beam are predominantly singly charged the landing energy is directly proportional to the landing bias such that 1 V = 1 eV=e = 1 eV/particle. The landing energy should ideally be kept < 1eV/atom also known as soft landing.[18] The soft landing regime is defined for nanoparticles and backed by experiments, which show the landing energy should be kept below the cohesive energy of the cluster[18] i.e. $E_{coh} > E_{landing}$ to avoid cluster fragmentation - although this depends on the substrate and cluster material. For small entities such as single atoms or dimers, these effects have not been experimentally investigated to the best of my knowledge. Figure 2.3 shows mass spectra of Pt single atoms and dimers at different landing biases.

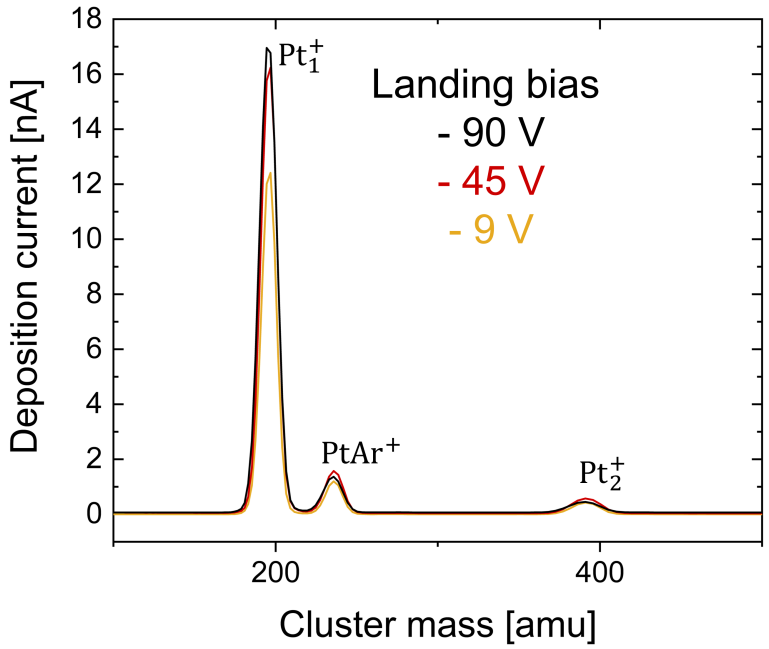

Figure 2.3: Effect of landing bias on the deposition current for Pt_1 and Pt_2. All entities are collected at 45 V. 9 V is used for depositions to approach the soft landing regime while maintaining a sufficient ion flux.

An increase of the landing bias increases the deposition current according to Ohm's law until all available entities are collected. To that end, the currents of Pt single atoms and dimers on figure 2.3 do not scale linearly, as the vast majority of entities are already collected 30 V. It is challenging to generate a sufficient flux of any small entitity larger than a single atom while maintaining a landing energy of 1 eV/atom. Therefore I decided to keep the landing energy at 9 eV/entity for the single atoms and dimers investigated in chapter 4.

Two of the previous PhD students (Jakob Ejler and Niklas Secher) who worked with the cluster source installed electric motors and made it possible to move the sample in a raster pattern during deposition. The rastering ensures a homogeneous deposition of clusters on the target substrate.[19;20]

2.2 Ion scattering spectroscopy

Low Energy Ion Scattering Spectroscopy (ISS) is a powerful surface analytical technique that provides information about the composition and structure of the outermost atomic layers of a solid surface. ISS is based on the scattering of low-energy ions (typically in the energy range of 100 eV to 10 keV) from a solid surface. The scattered ions are detected and their energy is measured at a known angle, providing information about the surface composition and structure.[21]

The ISS technique exploits the two-body collision of classical mechanics to derive the relation between the surface mass and the energy of the scattered ion given as

$$E_1 = \left(\frac{(M_s^2 \quad M_i^2 \sin^2 q)^{1=2} + M_i \cos q}{M_s + M_i} \right)^{\#_2} E_i \qquad (2.2)$$

where E_1 is the energy of the scattered ion, E_i is the energy of the incoming ion, M_s is the mass of the surface atom, M_i is the mass of the incoming ion and the scattering angle q. Hereby, if one uses an ion source such as 1 keV He^+, both the energy and mass of the incoming ion is known. The hemispherical analyser, which measures the energy of the outgoing ion E_1 is placed at a known angle relative to the substrate and ion source and makes

it possible to calculate the mass of the surface atom from which the ion has scattered. Only ions that retain their charge are measured in the analyzer. This means the ISS spectrum generated reflects the surface composition of the outermost atomic layer, as it is improbable for ions enterting the target substrate to keep their charge.[22] This makes ISS an extraordinarily useful tool for catalyst characterization, as the surface of the catalyst determines its catalytic ability. Lastly, since ISS only measures the outermost atomic layer, it can identify the presence of elements that are otherwise not detectable with techniques such as XPS, which under normal conditions probe at least 10 nm into the material and thus cannot detect a change in 1 atomic % to the surface alone.[22] This makes ISS a valuable tool when exploring low loading 2D samples, such as Pt single atoms on highly oriented pyrolytic graphite (HOPG), since XPS can not detect these small loadings.

2.2.1 Resolution and example spectrum

Due to the physics of the two body collision, heavy surface atoms will cause the scattered ion to maintain most of its kinetic energy. When M_S=M_i grows, the energy loss decreases logarithmically leading to a low resolution at high surface masses relative to the incident ions.

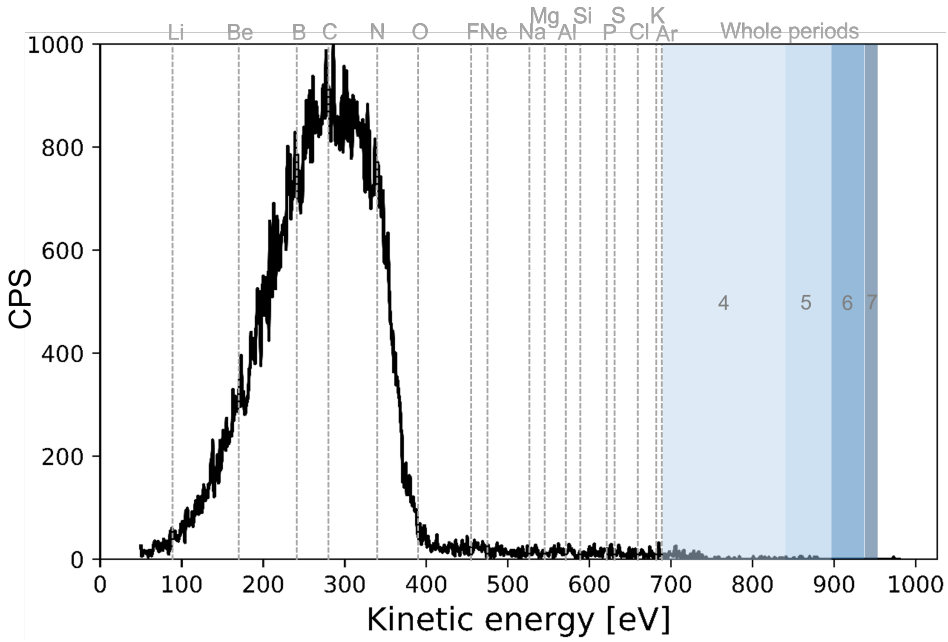

Figure 2.4: ISS spectrum of a clean HOPG crystal. Ion source is 1 keV He^+ and the detector angle is 146.7°.

Only noble gasses are suited to be used as incident ions, as other elements could react with the substrate and change its composition. Using a heavier noble gas increases the resolution but has the downside of increased surface sputtering. Figure 2.4 shows an example spectrum of an HOPG crystal after flash annealing at 1600 K, producing a very clean surface. The ion source is 1 keV He^+ and the detector angle is 146.7°, which is used throughout the thesis. The stippled lines represent the theoretical position of the different elements, while the colored blocks represent whole periods in the periodic table. Periods 6 and 7, which contain dozens of different elements each are resolved within about 10-20 eV. The broadening of the

carbon peak is caused by elastic losses, spread in energy from the source ion etc.[21] and means ISS is not suited to investigate the composition of an unknown sample, since neighboring elements heavier than Ar will be hard/impossible to distinguish.

2.2.2 Precision and peak scaling

In this thesis spectra will be shown of Pt nanoparticles, single atoms and dimers at different surface coverages. Therefore I will briefly show the expected precision and scaling behavior of the ISS technique.

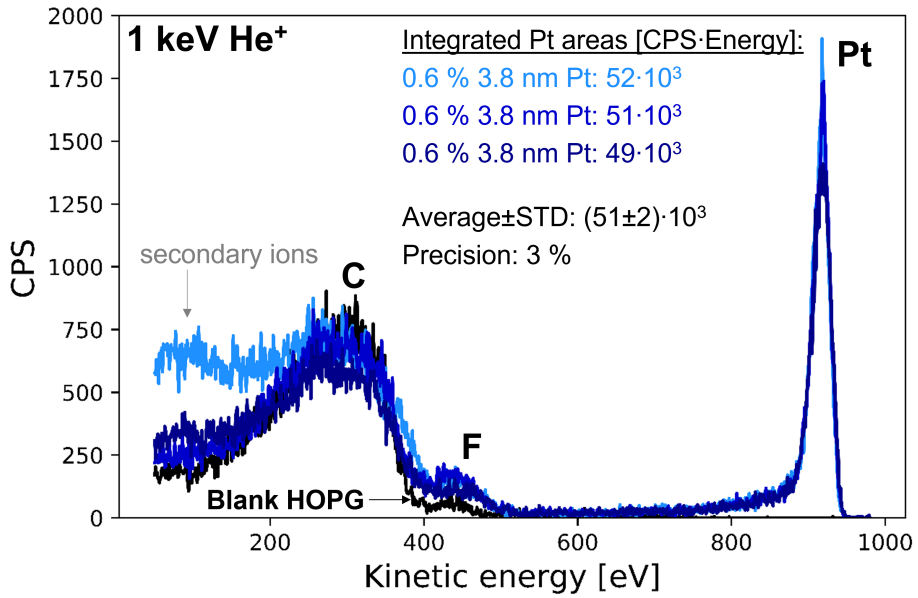

Figure 2.5: ISS spectra of a clean HOPG cystal (black) and three identically prepared HOPG crystals; each with 0.6 % projected coverage of 3.8 nm Pt. The integrated Pt areas are shown along with the average and standard deviation.

Figure 2.5 shows the ISS spectra of a clean (blank) HOPG co-plotted with three identically prepared HOPG crystals with 0.6 % coverage of 3.8 nm Pt nanoparticles, deposited using the cluster source. Moving from left to right, a secondary ion signal stemming mostly from adventitious carbon is

present at low energies for one sample. C, F and Pt signals are detected. Fluorine is present in trace amounts in our UHV system and sometimes adheres to the surface in minuscule amounts. By integration of the peaks, the precision is found to be 3 % for these experiments, but more generally a precision of 10-20 % is realistic. Pt scatters the He^+ ions much more efficiently than C as Pt only constitutes 0.6 % of the projected surface. This is caused by the difference in the elements ability to neutralize the incoming He^+ ions.

Generally, the signal in ISS (CPS) is given as

$$\mathrm{CPS} = \frac{S_i}{t} = \frac{I_p}{e} x R n_i N_i \tag{2.3}$$

where S_i is the ion yield, t is the acquisition time, I_p is the ion beam current hitting the sample, e is the elementary charge, x is an instrument factor, R is the roughness and shielding, n_i is the elemental sensitivity and N_i is the surface concentration of species i.[23]

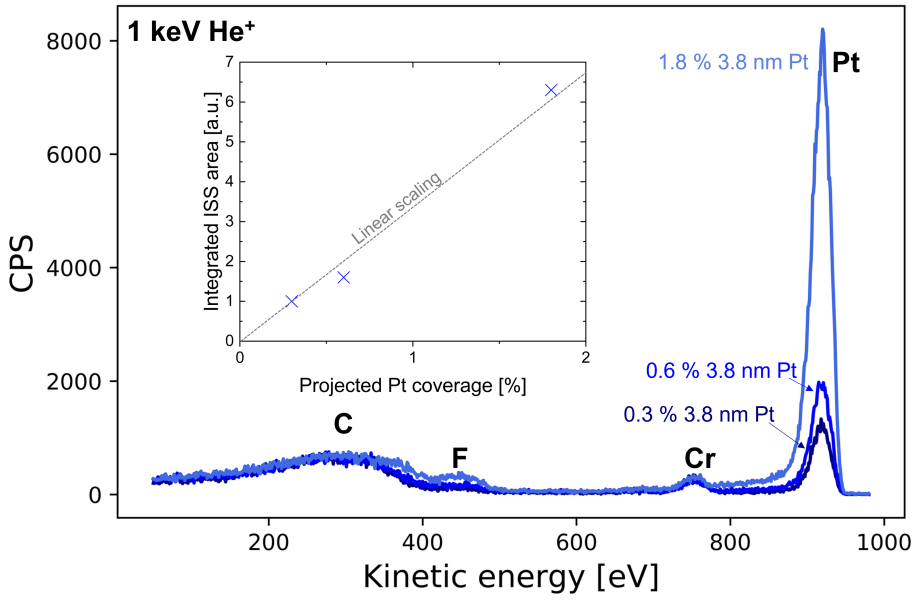

Figure 2.6: 3.8 nm Pt nanoparticles on HOPG at three different coverages. The inset shows the linear scaling of the integrated peak areas.

If the same experimental parameters are used, and the same element at low coverage (where roughness is minimal) is investigated, the relation can be reduced to

$$\frac{S_i}{t} = kN_i \tag{2.4}$$

with all the constants contained in k. For samples with different surface concentrations of the same element, but otherwise identical, the integrated peak areas should scale linearly. This linear scaling is evident from figure 2.6, where three different coverages of 3.8 nm Pt of 0.3 %, 0.6 % and 1.8 % on HOPG are shown. The inset shows the integrated Pt peak areas, which are seen to adhere close to perfect linearity. The integrated areas are normalized to the 0.3 % coverage.
Also present at the surface is Cr, which stems from a thermocouple mounted at the surface to monitor the annealing temperature. The linear scaling is only applicable to cases with entities that have the same neutralization probability, which is related to the electronic structure of the material.[23]

2.3 Scanning probe microscopy

Scanning probe microscopy are a class of microscopy techniques which use a physical probe to scan the surface of a sample. The techniques used in this project are atomic force microscopy and scanning tunneling microscopy.

2.3.1 Atomic force microscopy

Atomic force microscopy (AFM) is a powerful tool used in nanotechnology and materials science for studying the surface topography and properties of materials at the nanometer scale. It is a type of scanning probe microscopy (SPM) that uses a sharp tip mounted on a cantilever to scan the surface of a sample. The tip interacts with the surface forces, which are then measured by detecting the deflection of the cantilever using a laser.[24] A schematic illustration of the AFM principle is shown in figure 2.7a. The surface has to be flat for the AFM to be effective, thus making HOPG an ideal substrate to investigate with this technique. Figure 2.7b shows an AFM image of an HOPG crystal, illustrating the ability of the instrument to detect individual and multiple steps on the surface.

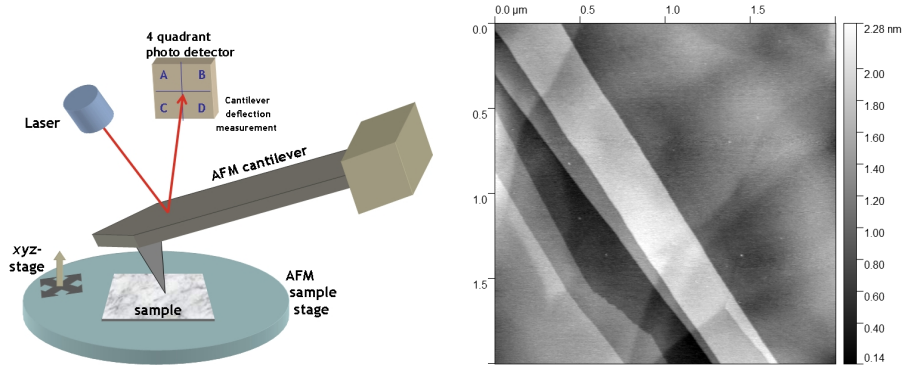

(a) **(b)**

Figure 2.7: (**a**) Schematic illustration of the AFM principle. Adapted from[25] under the CC BY 4.0 license. (**b**) (2 x 2) µm AFM image of a stepped HOPG crystal. Data acquired by Rikke Tankard.

2.3.2 Scanning tunneling microscopy

Scanning tunneling microscopy utilizes an atomically sharp tip to generate a tunneling current between the sample and the tip. A bias, V_t, applied to the sample cause a net flow of electrons, I_t, from the tip to the sample or vice versa depending on the sample polarity. Since the tunneling current is exponentially dependant on the tip to sample distance D it is possible to achieve atomic resolution is this manner.[26] Figure 2.8a shows a schematic of the STM principle. The generated image is a convolution of geometric and electronic structure at the fermi level, which poses a challenge in the interpretation of the images, as will become apparent in chapter 4.

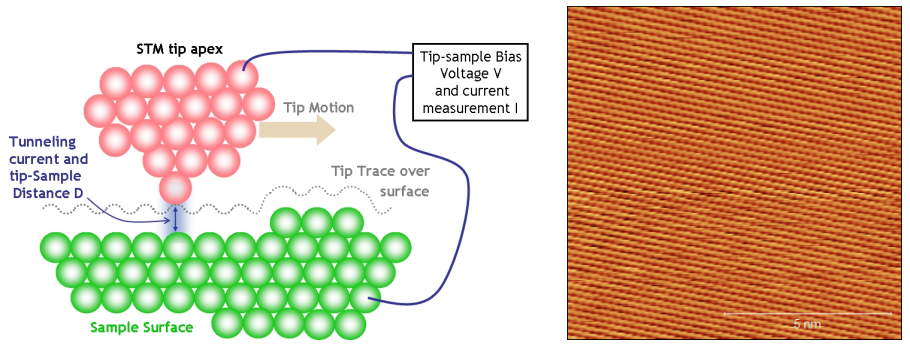

Figure 2.8: (**a**) Schematic illustration of the STM principle where an atomically sharp tip sits at a distance D and scans the surface.Adapted from[25] under the CC BY 4.0 license. (**b**) (10 x 10) nm STM image of an HOPG crystal. $V_t = +1\,\mathrm{V}$ and $I_t = 0{:}3\,\mathrm{nA}$. Image acquired by Miriam Galbiati.

Figure 2.8b shows an STM image of an HOPG crystal illustrating the hexagonal lattice of the HOPG crystal. Like the AFM technique STM requires a flat substrate. However, the tip of STM is a lot more sensitive to perturbations, as it has to maintain atomic sharpness to generate a usable image.

2.4 Rotating disk electrode

The rotating disk electrode (RDE) is a widely applied tool for the study of electrocatalysts. It consists of a rotating disk electrode, e.g. a glassy carbon

electrode, immersed in an electrolyte solution and connected to a potentiostat. By rotating the electrode at high speeds, typically around 1600 rpm., the forced convection of the electrolyte greatly increases the mass transfer of reactants and products to and from the surface of the electrode, where the catalyst of interest is deposited. Figure 2.9 shows a cross-sectional view of the RDE-setup.

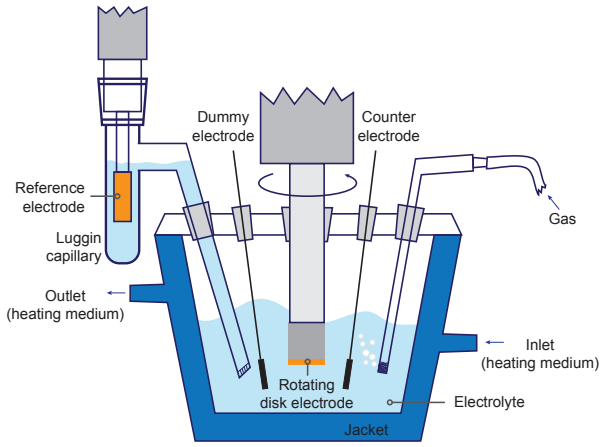

Figure 2.9: cross-sectional view of the rotating disk electrode setup. Image courtesy of Taus Holtug.

The reaction of interest takes place at the RDE (working electrode), whereas the complementary oxidation or reduction reaction takes place at the counter electrode. The reference electrode establishes the potential of the half reaction, which takes place at the working electrode. The dummy electrode is used to establish the potential of the working electrode prior to electrolyte contact to avoid the open circuit potential, which may harm the catalyst in question.

2.4.1 Potential scale calibration

In order to compare electrochemical reactions such as the hydrogen evolution reaction it is necessary to have a universally agreed upon scale. One widely used reference electrode is the standard hydrogen electrode (SHE), defined by the equilibrium $2H^+ + 2e^- \;) \; * \; H_2$ at activity $a_+ = 1$ and H_2

pressure of 1 bar. By definition this reference point has $E^0 = 0$ at all temperatures. Since the water splitting reactions involves the transfer of protons, their equilibrium potentials undergo a Nernstian pH-dependent shift at an identical rate of 0.059 mV per unit of pH. The reversible hydrogen electrode takes this into account by defining the HER/HOR equilibrium potential to be 0 V vs. RHE for all pH values. Practically, this means that the RHE scale can be used for different electrolytes, which makes it easier to compare measurements. This requires a careful calibration of the reference electrode, such that the equilibrium potential of the HER/HOR is $E^0_{\text{HER=HOR}}$ 0. This can only be achieved when the electrolyte is *continuously* saturated with H_2. A miscalibration of 20 mV of the RHE scale can easily result in a two-fold activity increase.[27;28;29] For the HER, a miscalibrated RHE scale typically shows as an HER current drawn at positive potentials vs. RHE. In this thesis all electrochemical potentials are given vs. RHE.

2.4.2 CO stripping

Platinum and platinum-like metals bind CO strongly. This can be exploited in electrochemistry using a method called CO stripping.

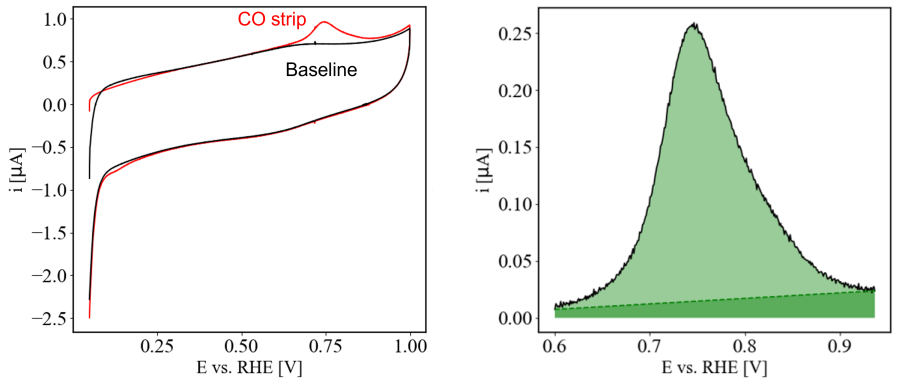

Figure 2.10: (**a**) Example of a CO strip (red) and baseline (black) measurement of 100 ng cm ^{2} 3.8 nm Pt on glassy carbon (**b**) Zoom in of CO strip peak. The light green area represents the strip charge and the dark green area is subtracted as additional background.

In brief, CO is dosed into the electrolyte while maintaining the WE at a positive potential of 50 mV vs. RHE. The electrolyte is purged with Ar to remove excess CO. Then the potential is cycled anodically and the CO is oxidized to CO_2 and escapes the surface, typically around 700 mV vs. RHE. In this way a CO strip peak is generated. After the CO strip cycle a baseline measurement is made with the same potential hold at 50 mV vs. RHE (without CO) to determine the background.
Figure 2.10a shows an example of a CO strip (red) and baseline (black) measurement of 100 ng cm^{-2} 3.8 nm Pt on glassy carbon. For low loadings and especially for monomers and dimers investigated in chapter 4, the baseline does not adhere closely to the CO strip peak. In these cases, an additional background was subtracted, highlighted by the dark green area under the stippled line on figure 2.10b. The cause of the baseline/CO strip cycle discrepancy is not fully understood, but might be caused by structural changes to the surface or an artefact of double layer capacitance. One way to explore this further is through electrochemical mass spectrometry, which would allow for a direct measure of the CO_2 released. However, this has not been pursued at this point.

Once the strip charge is known, it can be related to the available surface area of the catalyst, the so-called electrochemically active surface area (ECSA) by multiplication with the surface charge density $q_{CO,Pt} = 420\,\mu C\,cm^{-2}$.

Chapter 3

Benchmarking the hydrogen evolution reaction in acid

The work in this chapter is based on the publication[30], which is appended in appendix 5. I was responsible for preparing and characterizing the cluster source samples. Niklas Secher assisted in the sample deposition when necessary and developed an algorithm simulating the particle overlap. Johannes Hartmann did the electrochemistry and was responsible for writing the paper. Hector Prats made the numerical diffusion model simulation of mass transport in RDE. Karen Chan, Jakob Doganli-Kibsggard and Ib Chorkendorff supervised the work at devised the idea. All contributed in the discussion and interpretation of results.

3.1 Introduction

Platinum is the most active catalyst for the acidic hydrogen evolution reaction (HER).[31;4] its scarcity has lead to a signi cant research effort spanning the last 15 years in an attempt to nd a replacement. Figure 3.1 shows the number of publications published every year for the last 50 years within the eld. While there has always been some interest since the 1980s, the eld has exploded in popularity since the early 2010s with almost 7000 publications in 2022 alone. The vast majority of these research efforts are focused on an earth abundant alternative relative to Pt, with MoS_2 and CoP constituting a signi cant portion.

Figure 3.1: Number of papers published with the hydrogen evolution field since 1970. MoS_2 and CoP constitute a large part of the research effort.

3.1.1 The h_{10} paradigm

Although progress has been made with the advent of MoS_2 and CoP catalysts, they cannot compete with Pt in terms of neither mass activity of turnover frequency. The research effort apparent from figure 3.1 has largely been focused on decreasing a figure of merit known as h_{10}, which is the overpotential needed to reach a geometric current density of 10 mA cm^{-2} [2,32,33,34,35]. The h_{10} parameter had its origin within the sub field of photocatalytic watersplitting and embodies the approximate current density expected for a 10 % efficient solar-to-fuels conversion device under 1 sun illumination [36]. While this figure of merit is well-defined, it fails to take the mass loading of the used catalyst into account, since the geometric electrode area and not the actual catalyst area is used as normalization parameter. Thus, simply adding more catalyst to the electrode will decrease the h_{10} value. This is due to the mass transport limitations of the HER in a standard RDE setup. This approach is not feasible for a real electrolyser since mass transport (and ultimately space in the catalyst layer) will limit the effectiveness of this strategy. In a way, the h_{10} figure of merit encourages excessive catalyst loading, as it lets researchers claim an increased effectiveness of the catalyst material they have chosen to test. Indeed, any material added to a

carbon electrode will increase its HER performance, as determined by the instant classic: "Will Any Crap We Put into Graphene Increase Its Electrocatalytic Effect?" by Martin Pumera et. al.[37]
The vast majority of the reported catalysts are measured using an RDE-setup, which is a quick way to obtain an HER measurement. Adverse experimental practices are abundant within the eld and generally lowers the usefulness of the reported measurements.[31] Some of the common pitfalls are described in the following.

3.1.2 Common pitfalls

Erroneous potential scale calibration
The agreed upon standard potential scale within the eld is the RHE scale. This scale is only well-de ned if hydrogen is supplied continuously into the electrolyte. If hydrogen is merely used to purge the electrolyte prior to the experiments or if Ar is used as saturation gas, an ill-de ned Nernstian shift in favor of the HER will entail.[38] This results in a non-negligible HER current on the order of 1 mA at positive RHE potentials, which is obviously counter to the RHE de nition.

Poor choice of counter electrode
The counter electrode produces the anodic reaction when performing HER experiments and must be stable in this potential range. Importantly, a Pt counter electrode should be avoided as it may corrode anodically and redeposit on the working electrode, which enhances the apparent activity of earth-abundant catalysts.[39;40;41]

Comparison to subpar reference measurements
In the literature, a 20 wt. % Pt/C commercial catalyst is often used as reference. The excessive loading of Pt will cause the corresponding mass activity to decrease, again due to mass transport limitations. In this way, the mass activity is arti cially lowered for the commercial catalyst and makes it appear as if the novel catalyst has a similar or higher mass activity.

Neglecting intrinsic activity assessment
Often the intrinsic catalyst activity is not assessed. While it is immensely challenging to determine the actual turnover frequency of a catalyst due to

the high complexity and sheer number of possible active sites, it is the only intrinsic activity metric. Even an average turnover frequency can serve to indicate the catalyst merits and would in many cases reveal the materials lack-luster HER performance.

Oversight of mass transport limitations
The HER is mass transport limited in RDE, which means assessment of kinetic parameters such as the Tafel slope is not possible[42]. There will always be limits to the mass transport rate for an electrochemical technique, but efforts should be made to minimize the mass transport limitations for any given setup.

With these pitfalls in mind it seems feasible to make a benchmark study of Pt for the HER. This study aims to highlight the best practises for experiments while emphasizing the importance of reporting intrinsic catalyst activity and move away from the η_{10} paradigm.

3.2 Overview and characterization

In order to provide a solid literature reference point and to highlight the best practises needed when reporting HER activity a wide range of Pt loadings were deposited using the cluster source and a standard dropcasting method. The wide range of loadings makes it possible for other groups to compare their catalyst activities directly to a well-de ned standard. The samples presented are all 3.8 nm Pt on glassy carbon in a loading range of (13-100000)ng cm^2. The loading range of (13-5000) ng cm^2 were made using the cluster source. Additional samples in the loading range (5000-100000) ng cm^2 were dropcasted using a commercial Pt/C catalyst with an average nanoparticle size of 3.8 nm i.e. the same average size as the cluster source nanoparticles.

3.2.1 Sample preparation and overview

The Pt samples presented in this project were made in three different ways:

1. Deposited with the cluster source in a (1 x 1) mm raster pattern

2. Deposited with the cluster source in a (4 x 4) mm raster pattern

3. Pt/C ink dropcasted directly on the electrode

The samples made with the (1 x 1) mm raster pattern ensures all particles land within the con nes of the electrodes in an area of $6\,mm^2$. This means that the measured deposition current is directly proportional to the number of nanoparticles on the electrode and gives a high accuracy wrt. the loading on the electrode. This also causes the local coverage to be beyond one monolayer for the high loading samples.

(a) (b)

Figure 3.2: (a) SEM image of the $5000\,ng\,cm^{-2}$ 3.8 nm Pt on glassy carbon, made with (1 x 1) mm raster pattern. Figure adapted from [30]. (b) Mass spectrum of the particles present in the aggregation zone before and after deposition during 2 hours. There is no signi cant change to the distribution.

To alleviate this, samples made with a larger (4 x 4) mm raster pattern with area $30\,mm^2$ were added for the highest loading samples. Figure 3.2a shows a SEM image of the $5000\,ng\,cm^{-2}$ sample. It is clear that all particles are within the con nes of the glassy carbon stub (electrode). Figure 3.2 shows a mass spectrum of the particles in the aggregation zone before and after deposition of the longest deposition time i.e. $5000\,ng\,cm^{-2}$ with the (4 x 4) mm raster pattern. There is no signi cant change to the distribution and a large ratio between the desired 3.8 nm nanoparticles and the

double mass (4.8 nm) is present. This should minimize the amount of double mass double charge particles that will escape the mass filter along with the (desired) single mass single charge.

Loading ng cm^{-2}		Q_{CO} µC	TOF at η = 15 mV #H_2 site^{-1} s^{-1}	η_{10} mV
13	1	0.30	3.1 10^{-2}	133
19	1	0.46	2.6 10^{-2}	115
50	3	1.4	1.1 10^{-2}	85
100	5	2.6	7.9 10^{-1}	61
17	1	0.42	2.4 10^{-2}	120
50	3	1.6	9.8 10^{-1}	83
100	5	3.1	7.3 10^{-1}	54
200	10	6.7	4.8 10^{-1}	41
200	10	5.0	5.8 10^{-1}	48
500	25	16	2.8 10^{-1}	35
500	25	15	3.6 10^{-1}	34
1000	50	28	2.2 10^{-1}	29
5000	250	110	9.0	20
565	28 (4 x 4) mm	19	4.7 10^{-1}	24
1000	50 (4 x 4) mm	45	2.4 10^{-1}	21
5000	250 (4 x 4) mm	150	1.3 10^{-1}	16
500	34 drop.	15	4.0 10^{-1}	30
1000	67 drop.	36	1.7 10^{-1}	30
5000	276 drop.	220	5.0	21
50000	2975 drop.	2800	3.0 10^{-1}	21
100000	5150 drop.	3300	4.0 10^{-1}	18

Table 3.1: Overview of the 3.8 nm Pt samples. The samples in the first block are made with the (1 x 1) mm raster. The two remaining bloacks are denoted either (4 x 4) mm for the large raster or drop. for the dropcasted samples. The error given for the cluster source samples is derived from the resolution of the time-of- flight mass filter.

To explore even higher loadings, a Pt/C was dropcasted directly on the electrode using a commercial Pt/C ink with an average particle size of 3.8

nm. An overview of all the samples can be seen in table 3.1 along with key metrics used in the following analysis. The error given for the cluster source samples is derived from the resolution of the time-of- ight mass lter.

3.2.2 ISS characterization

The samples made with the cluster source were sputtered cleaned with 1 keV Ar^+ ions and characterized with ISS before and after deposition to ensure cleanliness of the substrates.

Figure 3.3: ISS spectra of all the different loadings made using the (1 x 1) mm raster. The Pt peak scales with loading. Inset shows the glassy carbon stub before deposition of Pt. Figure adapted from [30] SI.

Figure 3.3 shows ISS spectra of all the different loadings made using the (1 x 1) mm raster. The Pt peak scales linearly with loading until the two largest

loadings, which is unexpected. This could be an effect of the surface structure changing signi cantly as the nanoparticles form a continuous layer. The inset shows a glassy carbon stub after Ar sputter cleaning but before deposition of Pt. Mo, Ar and O is present at the surface. The trace amounts of Mo has likely migrated from the Mo sample holder onto the substrate. The Ar stems from the sputter cleaning and is probably physisorbed as it is an ideal inert gas. The oxygen is inherent to the glassy carbon substrate.

3.3 Assessing the electrochemically active surface area

In order to determine the intrinsic activity, i.e. the turnover frequency, it is necessary to the determine the number of active sites. For Pt, this can be done using the CO strip method[43]. Using this method, the total area participating in the electrochemical reaction can be determined. The CO strip charge measured for all samples can be seen in table 3.1. In order to assess whether the measured strip charge is inline with the expected value, two different tting methods were attempted.

3.3.1 Assuming the particles are spheres

The simplest way to create an expected value, is to assume the Pt nanoparticles behave as spheres. From this, the expected strip charge can be found based on the loading L, electrode area A_{geo}, radius of the nanoparticle $r_{particle}$, bulk density ρ_{Pt} and the surface charge density $s_{CO;Pt} = 420\,\mu C\,cm^{-2}$ as

$$Q_{CO}(L) = \frac{3A_{geo}Ls_{CO;Pt}}{r_{particle}\rho_{Pt}}$$

This assumes that the nanoparticles are perfect spheres and that their entire surfaces are exposed. Figure 3.4a shows the CO-strip charge of the (13-5000) $ng\,cm^{-2}$ loadings, with the expected CO-strip charge from the spherical approximation. Evidently, the spherical approximation overestimates the CO-strip charge. The linear t of the low loadings is consistent with a half sphere approximation. This could be due to loss of surface area to the support or because the surface charge density used overestimates the

charge released per area of Pt. Likely it is a combination of both, since the Pt sits of a glassy carbon stubs, meaning some of the Pt will not be exposed to the electrolyte. Furthermore, the surface charge density depends on CO adsorbtion potential, electrolyte and Pt surface structure and will likely be lower than $s_{CO;Pt} = 420\,\mu C\,cm^{-2}$.[44;45;46]

(a) (b)

Figure 3.4: (a) CO-strip charge of (13-5000) $ng\,cm^{-2}$ loadings. Inset shows a zoom of the lowest loadings. The spherical approximation overestimates the total strip charge. The linear fit aligns with a half sphere approximation. Simulated CO strip charge is made for the (1 x 1) mm raster. (b) CO-strip charge of all samples. Commercial Pt/C and (4 x 4) mm raster samples have a systematically higher strip charge than the (1 x 1) mm raster. Figure adapted from[30].

3.3.2 Numerical simulation

Another factor which impacts the CO-strip value is the particle overlap. In an attempt to get an idea of the magnitude of this effect, a simulation was made. The developed algorithm simulates a number of spherical 3.8 nm particles in an (x,y)-plane. If the spheres are within a certain distance of each other (< 0.3 nm) one of the particles is extended into the z-direction until it is edge to edge with the neighboring particle. The surface area is then found and a given value is subtracted for all particles that are edge to edge. Furthermore, an additional area is subtracted for the particles is the z

= 0 plane, to account for the area blocked by the support.
In order to determine the effect of the area lost due to the support, the simulation is first fitted to the low loading samples, where particle overlap is negligible as the coverage is on the order of 1-5 %. The area lost due to particle overlap is then found by fitting the entire range of loadings. In order to avoid over fitting, only the (1 x 1) mm raster samples are used in the simulation. This simulation accounts for the CO-strip charge of the cluster source samples, even at the highest loading of 5000 ng$_{Pt}$/cm^2, where the linear fit (roughly half sphere) does not accurately predict the CO-strip charge. A more detailed description of the simulation can be found in the SI.[30]

3.4 HER activity for different loadings

Now that all samples are accounted for and the electrochemical surface area has been measured, the gures of merit and the pitfalls they inherit are laid out. All measurements were done in N_2-saturated electrolyte of 0.5 M H_2SO_4 at a rotation rate of $\nu = 1600$ rpm.

3.4.1 Geometric current density

The most widespread way to assess HER activity is through the geometric current density i.e. the measured HER current divided by the geometric electrode area, typically given as $mA\,cm^{-2}$.

Figure 3.5: Geometric current density of selected cluster source (blue) and commercial (red) Pt/C samples. The η_{10} gure of merit is reduced for larger loadings, even though the samples are otherwise identical. Inset shows a zoom of cathodic and anodic sweeps, which should be centered aroud 0 vs. RHE on a properly calibrated RHE scale, with negligible current of $0{:}1\,mA\,cm^{-2}$ at $E = 0$. Figure adapted from[30].

As discussed, the figure of merit used, η_{10}, is the overpotential needed to reach 10 mA cm^{-2}. This fails to take the number of active sites into account and is easily reduced by simply adding more catalyst i.e. increasing the mass loading. Figure 3.5 shows the geometric current density for selected cluster source (blue) and dropcasted Pt/C samples (red). It is clear, that the η_{10} metric is reduced for the larger loading sample. This is seen for both the cluster source and commercial Pt/C samples and is purely an effect of increased loading, since all other parameters were constant for the two measurement series.
The inset shows a zoom of cathodic and anodic sweeps, which should be centered aroud 0 vs. RHE on a properly calibrated RHE scale, with negligible current of -0.1 mA cm^{-2} at $E = 0$.
Due to these considerations, it is meaningless to use η_{10} to account for increased catalyst activity when the mass loading is neglected.

3.4.2 Mass activity

(a) (b)

Figure 3.6: (a) Mass activity of the lowest and highest loading cluster source samples. The low loading sample outperforms the high loading sample due to mass transport limitations. (b) Mass activity of all samples; (1 x 1) mm raster (blue), (4 x 4) mm raster (green) and commercial Pt/C (red) all measured at 10 mA cm^{-2}. Figure adapted from [30].

Another widely used metric for the HER activity is the mass activity given as A mg^{-1}. Like the geometric current density, one needs to be aware of

the mass loading when reporting this figure of merit. Figure 3.6a shows the difference in mass activity for the lowest and highest loading cluster source samples. Given an overpotential of 25 mV the 5000 ng$_{geo}$ cm^{-2} sample delivers a mass activity of 3 A mg^{-1} whereas the lowest loading sample reaches 70 A mg^{-1}. Thus, increasing the mass loading of the catalyst on the electrode will cause the mass activity to plummet.

Figure 3.6b shows the mass activity against the overpotential, both given at 10 mA cm^{-2} of geometric current for all samples. The blue and green dots show the small and large raster pattern respectively, while the red dots show the commercial Pt/C. This plot also confirms, that the η_{10} parameter can be decreased by increasing the mass loading. This is a testament to the relation $j_{mass} = j_{geo} \cdot \text{Loading}^{-1}$. The consequence of these findings are severe when the mass activity of novel HER catalysts are reported while referencing a commercial 20 % Pt/C catalyst sample - as often seen in the literature.[47;48] This fallacy artificially suppresses the mass activity of the referenced Pt/C sample as the mass transport limitation of the RDE-technique limits the production of hydrogen. In this way, it is possible to measure a higher or comparable mass activity than Pt of a novel HER catalyst.

3.4.3 Turnover frequency

The turnover frequency (TOF) i.e. $\#_{H_2}$site^{-1}s^{-1} is the only way to determine the intrinsic activity of a catalyst. While the mass activity is important from a techno-ecomic standpoint, since elements are paid for by mass, the turnover frequency is the scientifically relevant figure of merit. The turnover frequency is calculated as

$$\text{TOF} \left(\frac{H_2}{\text{site s}} \right) \qquad \text{TOF} = \frac{i / q_{HER}}{Q_{CO} / q_{CO}} = \frac{i}{Q_{CO}}$$

where, i is the HER current, Q_{CO} is the measured CO-strip charge and q_{HER}/q_{CO} is the charge transfer of the HER and CO-strip reactions. The HER and CO-strip are both 2-electron reactions, meaning the TOF reduces to the HER current divided by the CO-strip charge.

Figure 3.7a shows the TOF for the different loadings at an overpotential of